AIAA JOURNAL
Vol. 39, No. 8, August 2001

Effects of Reflected Light in Luminescent Paint Measurements

Wim Ruyten* and Charles J. Fisher†
Sverdrup Technology, Inc., Arnold Air Force Base, Tennessee 37389-4300

A theoretical model is described that may be used to calculate the effects of reflected light in luminescent paint measurements. The key assumption of the model is that the paint may be treated as a diffuse reflector at the paint's emission wavelength. This allows the application of techniques that have been developed in the fields of radiative transfer and computer graphics to the present problem. A numerical example is considered to demonstrate that, in a pressure-sensitive paint test on a Dornier Alpha jet, the self-illumination effect at the paint's emission wavelength can produce pressure errors of up to 3% of actual pressure. However, it is also shown that a correction of this error is possible. This correction calls for mapping image data to a three-dimensional grid of the test article and calculating, at each element of the three-dimensional grid, the combined reflected light contribution from all other elements on the grid. An algorithm is described for the calculation of the required influence coefficients, including the detection of occlusions.

I. Introduction

LUMINESCENT paint measurements have become an important new tool for mapping global distributions of pressure or temperature (or both) on aerodynamic test articles.[1–4] In such measurements, a short-wavelength source is used to illuminate the test article, and the long-wavelength emission from the paint is imaged by one or more cameras (see Fig. 1). Given the dependence of the luminescent yield on pressure (strictly speaking, on oxygen density at the surface) and temperature, it is then possible to construct a map of the pressure or temperature distribution on the surface of the test article.

Broadly speaking, luminescent paint measurement can be divided into two categories: intensity-based methods and lifetime-based methods. In intensity-based methods, images of the test article are taken at the actual test condition and a known reference condition, for example, 1 atm. Data processing is then based on the ratio of the signals at the reference and test conditions to remove effects of nonuniform illumination and nonuniform paint thickness. In lifetime methods, measurement is based on ratioing two signals that are both taken at the actual test condition, but at different times following pulsed (or modulated) illumination of the paint. In this manner, a measure of the fluorescence lifetime is obtained, independent of illumination level and paint thickness. The measured lifetime is then converted to pressure or temperature.[5,6]

The purpose of this paper is to address an artifact that arises in both intensity-based and lifetime-based luminescent paint measurements. This is the effect of reflected emission light. In particular, we consider what happens if emission light from one part of a test article is reflected by another part of the same test article (see Fig. 2). As will be seen, such self-illumination produces a measurement error that is not compensated by the ratioing techniques just described.[7,8] As will also be seen, it is possible to perform a numerical data correction that minimizes this self-illumination error.[8,9]

II. Diffuse Reflection Model

The effects of self-illumination depend on a host of factors including the geometry of the test article, the pressure or temperature distribution on the surface, the reflective properties of the paint, and (in the case of nondiffuse reflection) the placement of the cameras relative to the test article. Here we consider the case in which the painted surface may be treated as a diffuse reflector in the sense that the distribution of reflected emission light is Lambertian. This term has a precise technical meaning,[10,11] but may be stated simply as follows: For a given spot on the surface of the test article, the brightness of the reflected emission light is independent of the direction of observation. Likewise, it is assumed that the emission process itself is Lambertian. Although the Lambertian, that is, diffuse, emission assumption is a good approximation for most paints, the assumption concerning the diffuse nature of the reflection process is not particularly accurate for glossy surfaces. These require an accounting of specular reflection in addition to diffuse reflection. In the most general case, the reflective properties of the surface would be described in terms of a bidirectional reflection distribution function.[10,12,13]

The reason for the choice of the diffuse reflection model in the present paper is twofold: First, it turns out to be a reasonable approximation for some of the important luminescent paints that are being used.[14] Second, it allows for a much simpler mathematical treatment than is required for a more complex reflection model.[10] Furthermore, the diffuse reflection model is one that has been used extensively in at least two other engineering disciplines: the study of radiative transfer[10,15] and computer graphics.[16,17] In computer graphics, the problem of rendering photo-realistic scenes of three-dimensional structures by computer has given rise to so-called radiosity techniques.[16,17] The important insight common to these different fields of study is that, for a diffusely reflecting surface, the total brightness L_i of a surface element ΔS_i may be written as the sum of an intrinsic brightness $L_i^{(0)}$ (the net emission term) and a reflected term that is related to the total (not the intrinsic) brightness values L_j elsewhere on the surface[10,16]:

$$L_i = L_i^{(0)} + R_i \sum_{j=1}^{N} \Delta F_{ji} \Delta S_j L_j \tag{1}$$

where R_i is the reflectivity of the surface element ΔS_i (a number between zero and unity), N is the number of surface elements, and ΔS_j is the area of the surface element that is producing the brightness L_j. The factors ΔF_{ji} are known as form factors, configuration factors, or view factors and are purely geometry dependent. Their calculation may be found in many texts on radiative transfer[10,15] and computer graphics,[16,17] as well as in Sec. III of this paper. Given a set of N intrinsic brightness values $L_i^{(0)}$, the calculation of the corresponding N total brightness values L_i from Eq. (1) is an implicit problem. Rather than solve the associated set of $N \times N$ linear equations directly (with N a number possibly as large as 10^5 or larger), it is usually preferable to solve Eq. (1) recursively, for example, using Jacobi relaxation (see Ref. 17). That is, given a set of N values $L_i^{(0)}$, successive sets of values $L_i^{(n)}$ (with $n = 1, 2, 3, \ldots$, and $i = 1, \ldots, N$) are calculated according to

$$L_i^{(n)} = L_i^{(0)} + R_i \sum_{j=1}^{N} A_{ij} L_j^{(n-1)} \tag{2}$$

Presented as Paper 2000-0833 at the AIAA 38th Aerospace Sciences Meeting, Reno, NV, 10–13 January 2000; received 27 January 2000; revision received 1 September 2000; accepted for publication 1 October 2000.

*Engineer Specialist, Technology Department; wim.ruyten@arnold.af.mil. Senior Member AIAA.
†Senior Engineer, Technology Department.

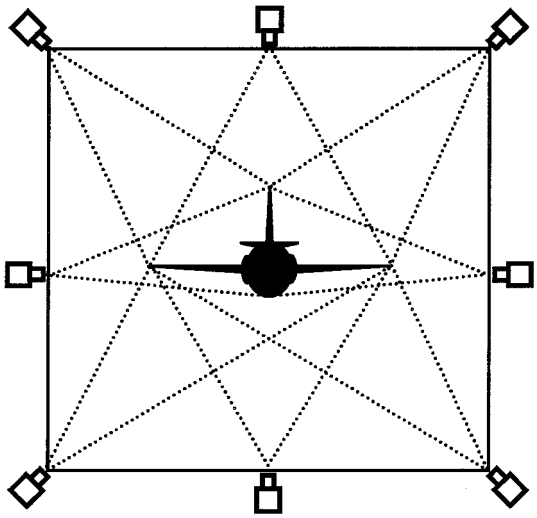

Fig. 1 Schematic of eight-camera PSP system in AEDC's 16-ft transonic wind tunnel.

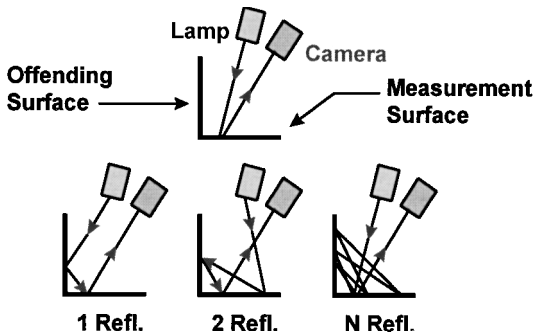

Fig. 2 Intended (top) and unwanted contributions (bottom) of reflected emission light to detected signal.

where the coefficients A_{ij} are defined as

$$A_{ij} = \Delta F_{ji} \Delta S_j \tag{3}$$

and may be thought of as the elements of a matrix $\boldsymbol{A}$. With each iteration, the set of values $L_i^{(n)}$ in Eq. (2) becomes a better approximation to the set of sought-after total brightness values L_i from Eq. (1). A slightly more efficient iteration known as Gauss–Seidel is obtained by performing the iteration from Eq. (2) "in place" (see Ref. 17), with a single array representing both the values $L_i^{(n)}$ and $L_j^{(n-1)}$. In either case, the iteration number n may be thought of as the number of reflection orders that is included in the calculation of the total brightness values.[8]

When Eq. (1) is rearranged, the intrinsic brightness $L_i^{(0)}$ is found as an explicit function of the total brightness distribution L_j:

$$L_i^{(0)} = L_i - R_{\text{em}} \sum_{j=1}^{N} A_{ij} L_j \tag{4}$$

In writing Eq. (4) it has been assumed that the reflectivity of the painted surface at the emission wavelength is uniform and is given by $R_i = R_{\text{em}}$. The result from Eq. (4) lends itself well to performing a self-illumination correction on luminescent paint data because the total brightness values L_i and L_j may be taken to represent the experimental signals, for example, counts per image pixel. Thus Eq. (4) suggests the following processing steps for reducing luminescent paint measurements, including a self-illumination correction:

1) Measure the reflectivity R_{em} of the paint at the emission wavelength, for example, using the technique described in Ref. 14.

2) Define a three-dimensional grid of the surface of the test article, consisting of N surface elements ΔS_i.

3) Calculate the $N \times N$ set of form factors ΔF_{ji} and the associated coefficients A_{ij} for this grid.

4) Map each set of image data onto the three-dimensional grid, yielding a set of N values L_i for each image.

5) Calculate, for each set of N values L_i, the corrected values $L_i^{(0)}$ from Eq. (4).

6) Use the corrected values $L_i^{(0)}$ to calculate signal ratios and convert to pressure or temperature in the usual way.

Note that this processing scheme calls for mapping image data onto a three-dimensional grid before calculating pressures or temperatures. This step may involve combining image data from multiple cameras onto a single three-dimensional grid. By contrast, in conventional processing of luminescent paint images, data are not mapped onto a three-dimensional grid until after two-dimensional pressure or temperature images have been obtained.

III. Calculation of Form Factors

Given the prevalence of the form factors ΔF_{ji} in the study of radiative transfer and in computer graphics, many techniques for their calculation have been published.[15] Fundamentally, the form factor ΔF_{ji} between two surface elements ΔS_i and ΔS_j at positions $\boldsymbol{x}_i$ and $\boldsymbol{x}_j$ (Fig. 3) is given by[10]

$$\Delta F_{ji} = \frac{\cos \vartheta_{ij} \cos \vartheta_{ji}}{\pi |\boldsymbol{x}_{ij}|^2} \tag{5}$$

where $|\boldsymbol{x}_{ij}|$ is the distance between the two surface elements (note that $\Delta F_{ji} = 0$ for $j = i$) and ϑ_{ij} and ϑ_{ji} are the angles between the line of sight between the two surface elements and the surface normals $\boldsymbol{n}_i$ at $\boldsymbol{x}_i$ and $\boldsymbol{n}_j$ at $\boldsymbol{x}_j$, respectively. Complications arise when the line of sight is occluded by some part of the surface being imaged. The more complex the three-dimensional shape of the test article, the more cumbersome can be the detection of such occlusions. The technique proposed here for the calculation of the form factors is one based on the unit-sphere projection method, proposed in 1928 by Nusselt (see Ref. 10). The implementation of this technique is as follows (Fig. 4): For a given surface element ΔS_i with surface normal $\boldsymbol{n}_i$, define a flat, circular map of radius R_{map} in the plane of ΔS_i. Circumscribe a spherical shell of the same radius around this map, whose apex is defined by the line that protrudes from the surface normal $\boldsymbol{n}_i$. Now perform the following two projections for each surface element ΔS_j that has a surface normal $\boldsymbol{n}_j$ and a line-of-sight

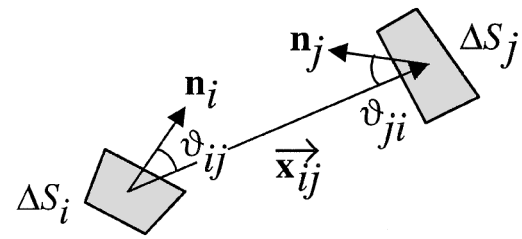

Fig. 3 Pair of surface elements of three-dimensional grid.

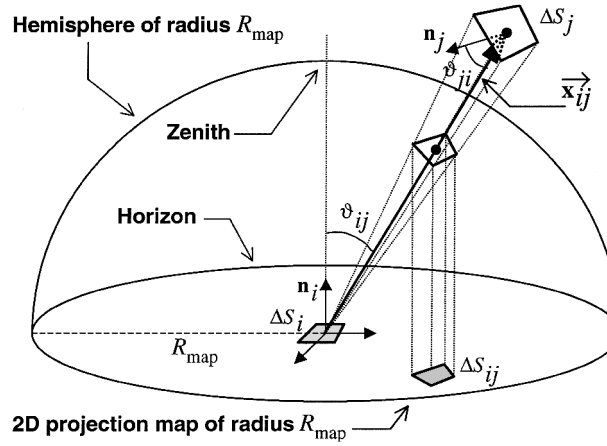

Fig. 4 *Z*-buffer implementation of Nusselt's method for calculating form factors.

vector $\boldsymbol{x}_{ij}$ for which both $(\boldsymbol{n}_i \cdot \boldsymbol{x}_{ij}) > 0$ and $(\boldsymbol{n}_j \cdot \boldsymbol{x}_{ij}) < 0$ (otherwise, the surface elements ΔS_i and ΔS_j do not face each other): 1) Project the surface element ΔS_j radially inward from the point $\boldsymbol{x}_i$ onto the spherical shell. 2) Project the resulting hemispherical element parallel to the surface normal $\boldsymbol{n}_i$ onto the flat, circular projection map. Let the area of the resulting element in the flat projection map be given by ΔS_{ij}. Then the coefficient A_{ij} from Eq. (3) (being the product of the form factor ΔF_{ji} and the original surface element area ΔS_j) is given by[10]

$$A_{ij} = \Delta S_{ij} \big/ \pi R_{\text{map}}^2 \tag{6}$$

That is, the coefficient A_{ij} is the ratio of the projected surface element area ΔS_{ij} and the area of the two-dimensional projection map. To detect occlusions, the two-dimensional circular map is discretized into a square array of pixels that has a pair of two-dimensional arrays associated with it: one that keeps track of the index j of a projected surface element for each pixel and one that, if a pixel has a surface element projected onto it, keeps track of the distance $|\boldsymbol{x}_{ij}|$ between the two surface elements ΔS_i and ΔS_j. When another surface element ΔS_j is protected onto the circular projection map, the decision whether this element is in front or behind a previously projected element (from the viewing perspective of the element ΔS_i) can now be based on a comparison of the previously recorded and newly calculated distances $|\boldsymbol{x}_{ij}|$. This technique for handling occlusions is well known in computer graphics as z buffer.[16]

Having projected, for a given surface element ΔS_i, all surface elements ΔS_j that are visible from ΔS_i, the task of calculating the areas ΔS_{ij} from Eq. (6) is reduced to the task of counting, for each surface element index j, how many pixels have been assigned to it in the z-buffer projection map. Specifically, let N_{ij} be this number of pixels for a projected surface element ΔS_j. Then the coefficient A_{ij} from Eq. (6) is given by

$$A_{ij} = N_{ij} \big/ \pi N_{\text{map}}^2 \tag{7}$$

where πN_{map}^2 is the total number of pixels in the circular projection map and N_{map} is the radius of the projection map, that is, the value R_{map} from Eq. (6) in pixels.

The stated implementation of Nusselt's method is similar to the hemicube method that has become commonplace for calculating form factors in radiosity calculations.[15–17] In it, the first of the two projections from Fig. 4 is performed onto a half-cube rather than a spherical shell. This has the advantage that straight-line segments of to-be-projected surface elements remain straight-line segments throughout the projection process. By contrast, straight-line segments become curved in the projection from Fig. 4. However, because three-dimensional grids for luminescent paint measurements are typically quite fine, it is postulated that this curvature may be neglected. The algorithm based on the hemispherical projection then has several advantages over the hemicube method. First, a simpler projection algorithm results. Second, the result of the calculations (the N_{ij} values) can be stored as integer rather than floating-point values. This allows for more compact storage of the implied A_{ij} coefficients than is possible for the hemicube method. This leads to reduced storage requirements (which can still amount to hundreds of megabytes per file) and processing time for performing the self-illumination corrections. Some of these computational issues are addressed in the Appendix.

IV. Simulation of Intensity-Based Pressure-Sensitive Paint Measurement

To illustrate the effects of self-illumination and how to deal with them, a numerical simulation is performed in Sec. V. This simulation assumes a pressure-sensitive paint (PSP) test that is based on the intensity method, as described in Sec. I. Specifically, it is assumed that image data for a test article are obtained at a uniform reference condition (wind-off) and at a wind-on measurement condition. For purposes of demonstration, the pressure distribution is assumed to be known in terms of a computational fluid dynamics (CFD) calculation. Also, it is assumed that the response of the paint can be described in terms of a linear Stern–Volmer relationship (see Ref. 18). (If desired, the model can easily accommodate additional nonlinear terms.) The pressure p_i on a surface element ΔS_i can thus be related to the intrinsic brightness $L_i^{(0)}$ of surface element ΔS_i according to

$$p_i = A + B\left\{\left[L_i^{(0)}\right]_{\text{wind off}} \big/ L_i^{(0)}\right\} \tag{8}$$

where A and B are calibration constants of the paint. Note that Eq. (8) implies an inverse relationship between pressure and brightness, with brightness increasing as pressure decreases, and vice versa.

Now consider the effect of reflected emission light. Measured signals are proportional to total brightness rather than net, intrinsic brightness. Use of total brightness values thus produces the modified pressure distribution p_i', given by

$$p_i' = A + B([L_i]_{\text{wind off}}/L_i) \tag{9}$$

The resulting pressure error is given by

$$\Delta p_i' = p_i' - p_i \tag{10}$$

with p_i the actual pressure and p_i' given by Eq. (9). In Eq. (9), it is assumed that the constants A and B are the same as those in Eq. (8), having been determined by some a priori calibration, for example, using painted coupons in a pressure- and temperature-controlled calibration chamber. In an alternative approach, the constants A and B may be determined using an in situ calibration involving pressure transducers embedded in the test article. In this case, Eq. (9) is used to fit measured brightness ratios in the immediate vicinities of the transducers to the pressure values from the transducers. Let the resulting fit coefficients be denoted by A'' and B''. When these coefficients are applied to other parts of the test article, the following pressures are obtained:

$$p_i'' = A'' + B''([L_i]_{\text{wind off}}/L_i) \tag{11}$$

The resulting pressure errors are now given by

$$\Delta p_i'' = p_i'' - p_i \tag{12}$$

Other calibration schemes are possible, in which only a single coefficient (not necessarily one of the coefficients A and B used here) is fit against the pressure transducer values, and the remaining coefficients are held fixed at the values from an a priori calibration.[19]

V. Numerical Example: Alpha Jet

To test the diffuse reflection model, the test article was taken to be one that has been previously tested in Arnold Engineering Development Center's (AEDC's) 16-ft transonic wind tunnel. This is the Dornier Alpha jet, also known as the Trans-Sonische Tragflügel (TST) model.[20] Figure 5 shows a CFD-generated surface pressure map for this model. Because of the high placement of the main wings, negligible self-illumination effects are expected for the upper part of the aircraft, which has a largely convex shape. By contrast, significant self-illumination effects may be expected in the vicinity of the joint line between the lower wing and the fuselage, due to the enclosing, concave nature of these two surfaces. This is borne out by the calculation of the coefficients A_{ij} from Eq. (3), which is discussed in the Appendix.

The intrinsic brightness distribution $L_i^{(0)}$ at the wind-off condition was assumed to be uniform (as would be the case for perfectly uniform lighting of the model surface) with one modification, which is the inclusion of self-illumination at the excitation wavelength. Unlike self-illumination at the emission wavelength, such self-illumination does not have an adverse effect on the outcome of luminescent paint measurements because it affects wind-off and wind-on measurements equally. Indeed, self-illumination at the excitation wavelength merely acts as a virtual light source that changes the illumination distribution on the test article. (Recall from Sec. I that ratioing is used precisely to compensate for effects such as nonuniform illumination.)

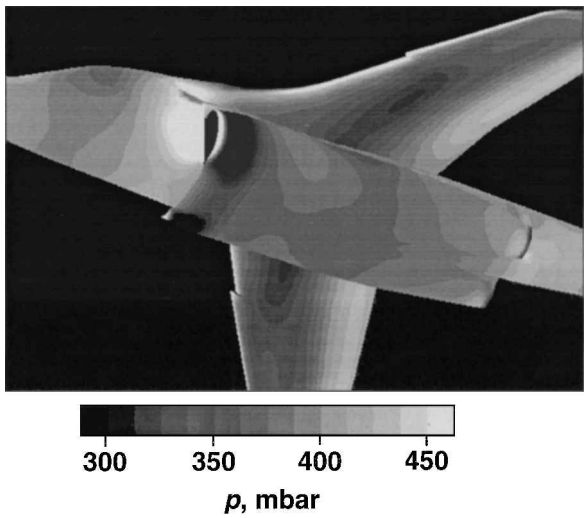

Fig. 5 Assumed pressure distribution on TST model.

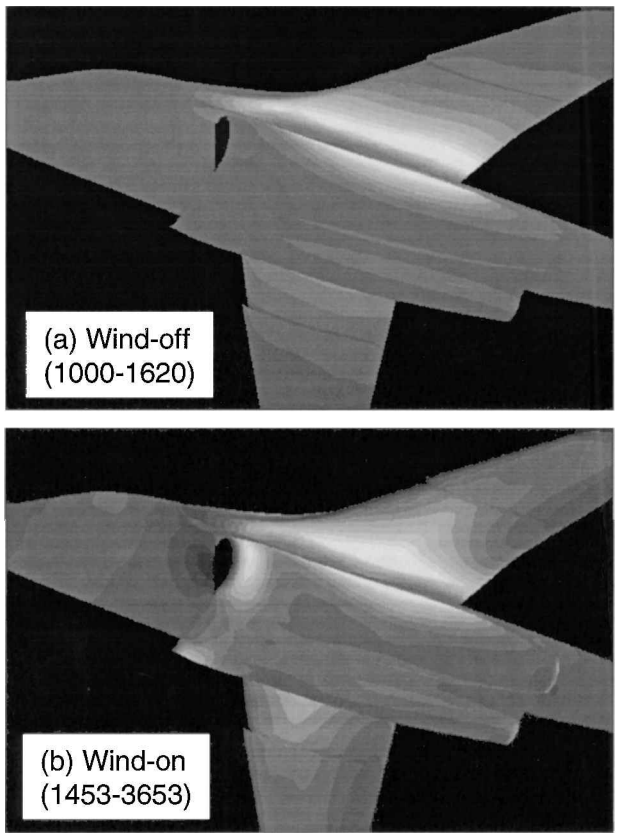

Fig. 6 Brightness distributions in absence of reflected emission light.

Figure 6 shows calculated brightness distributions on the test article that include the effects of reflected excitation light, but not those of reflected emission light. This calculation was performed using Eq. (2), setting $L_i^{(0)} = 1000$ at all surface elements ΔS_i, and using a reflectivity $R_i = 0.6$. Convergence to within machine precision was reached after 18 iterations. Figure 6 shows the resulting wind-off and wind-on brightness distributions. Minimum and maximum brightness values are shown in parentheses. The wind-on brightness distribution in Fig. 6b was calculated from Eq. (8) using data from Figs. 5 and 6a as input. Values of the paint coefficients A and B were taken to be given by $A = -184.6$ mbar and $B = 1164.5$ mbar, as is approximately the case for the PSP FIB7 used at AEDC. Maximum brightness values in Fig. 6 are about twice as large as would be the case in the absence of reflected excitation light.

Figure 7 shows the brightness distributions that are obtained after including the effect of self-illumination at the emission wavelength as well. Again, Eq. (2) was used, setting $L_i^{(0)}$ to the calculated distributions from Figs. 6a and 6b, respectively. This time, a reflectivity of $R_i = 0.79$ was used. This is the measured reflectivity of FIB7 at the emission wavelength.[14] Convergence to within machine precision was reached in 21 iterations. As is the case in Fig. 6, minimum and maximum brightness values are shown in Fig. 7. Maximum values are now up to four times larger than would be the case in the absence of reflected light.

A Priori Calibration

We are now ready to consider the effect of self-illumination on the calculation of PSP-derived pressure distributions. First, we consider the case of an a priori calibration. In this case, Eq. (9) is used to convert the total brightness distributions from Fig. 7 to pressures.

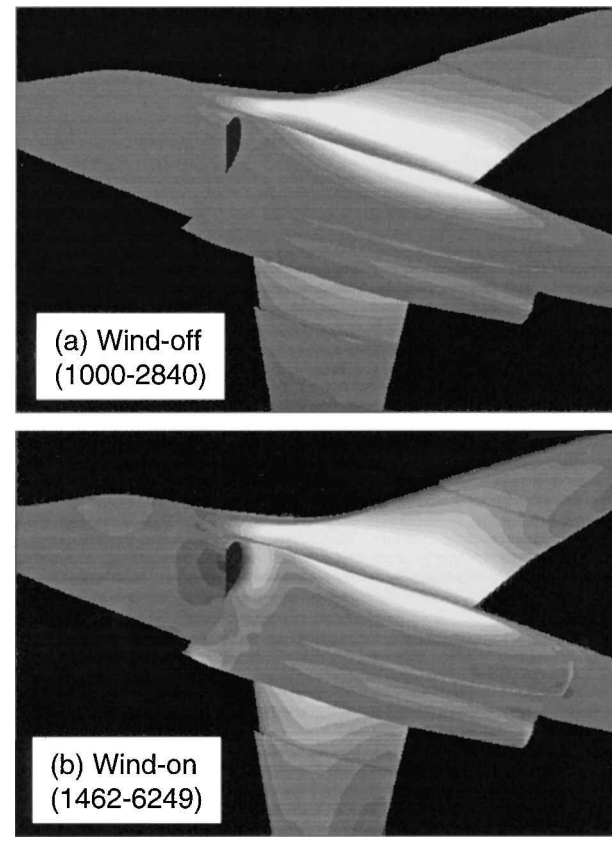

Fig. 7 Brightness distributions with reflected emission light included.

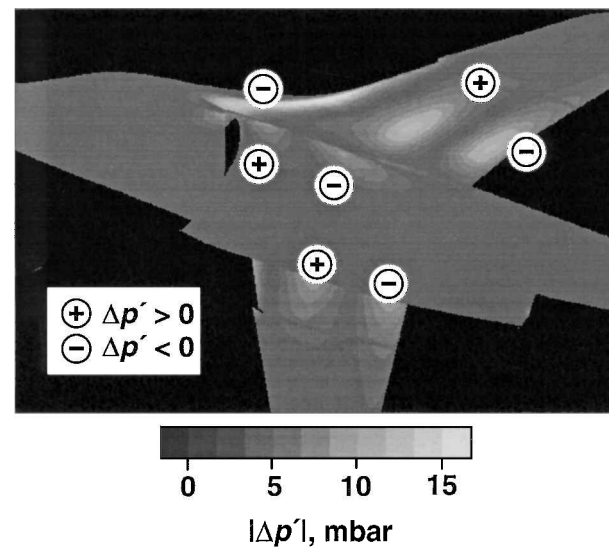

Fig. 8 PSP-pressure errors in absence of self-illumination correction for a priori calibration.

The associated pressure errors are then given by Eq. (10). Figure 8 shows these errors in image format. Minus and plus signs are used to indicate the signs of the errors. Figure 9 shows line plots of the same errors at three wing-span locations (21, 50, and 76%) on the lower part of the main wing. Maximum errors are seen to amount to about 15 mbar, or about 3% of the actual pressure. As expected, significant errors are found only in those areas in which geometry is such that there is significant self-illumination. However, to produce a self-illumination error, a second condition must be satisfied, namely, that there be a significant nonuniformity in the pressure distribution.[8] This explains why the extent of the isolated regions of pressure error in Fig. 8 is much more confined than the regions of high self-illumination in Fig. 7 and why the maximum relative pressure error (3%) is much smaller than the factor (see Figs. 6 and 7) by which the maximum brightness is increased as a result of self-illumination.

As a check, the self-illumination correction from Eq. (4) was applied to the data from Fig. 7. This reproduced, to within machine precision, the brightness distributions from Fig. 6 and, hence, by application of Eq. (8), the same pressure distribution that was initially assumed in Fig. 5.

In Situ Calibration

In a second calculation, it was assumed that, at each of the three span-wise locations from Fig. 9, a row of 15 equally spaced pressure transducers was located. Figure 10 shows a simulated in situ calibration based on readings from these transducers, with $L^{(0)}/L$ representing the wind-off/wind-on brightness ratios at the transducer locations derived from the PSP measurement. (These brightness ratios were calculated without performing a self-illumination correction.) Fitting the data from Fig. 10 to Eq. (9), the values $A'' = -221.2$ mbar and $B'' = 1244.0$ mbar were obtained. For comparison, the dashed line in Fig. 10 represents the result of the a priori calibration, with

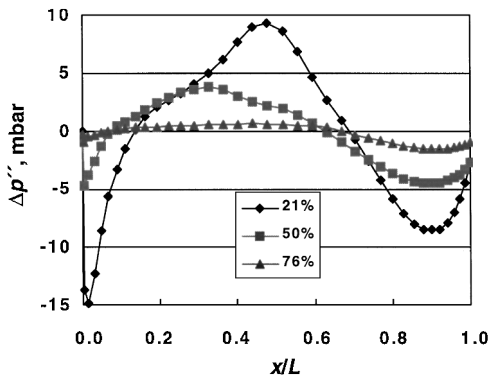

Fig. 9 Chordwise PSP-pressure errors on lower wing for a priori calibration.

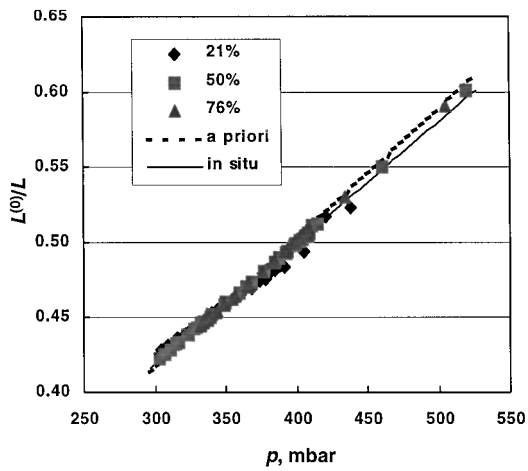

Fig. 10 In situ calibration on lower wing.

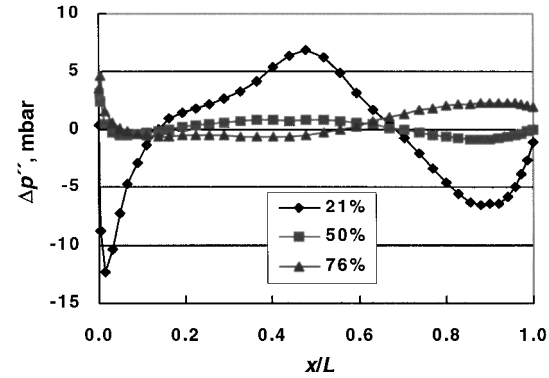

Fig. 11 Chordwise PSP-pressure errors on lower wing for in situ calibration.

$A = -184.6$ mbar and $B = 1164.5$ mbar. When the results of the in situ calibration are used, the brightness values from Fig. 7 were converted to pressures using Eq. (11). Figure 11 shows the resulting pressure errors from Eq. (12) at the same wing-span locations that are shown in Fig. 9. When the pressure errors in Fig. 11 are compared to those in Fig. 9, it is seen that only a slight improvement in the resulting pressure errors is obtained. Thus, it follows that the in situ calibration is not an effective means of correcting for reflected emission light. This result is not surprising because no single adjustment of the paint coefficients A and B can reasonably be expected to compensate for an artifact (self-illumination) whose influence is highly position dependent.

VI. Conclusions

Using a simple model, it has been shown that reflected light in luminescent paint measurements can triple the brightness of selected surface areas on a test article, compared to the case of no reflection. In both intensity-based and lifetime-based methods, signal ratioing compensates for this effect. This compensation is complete for reflected excitation light, but not for reflected emission light. As shown, the associated pressure error in a PSP measurement can reach several percent of actual pressure. However, as is also shown, a self-illumination correction can be performed to reduce this error. This calls for mapping image data to a three-dimensional grid of the test article and calculating at each point on the grid a correction term that involves measured image data from, in principle, all other points on the grid. The computational effort associated with such a calculation is proportional to N^2, where N is the number of surface elements on the grid. By contrast, the computational effort associated with conventional processing of luminescent paint data is proportional to N. A self-illumination correction thus poses a significant additional computational burden.

In the numerical example studied here, the accuracy of the proposed self-illumination correction is limited only by machine precision. In practice, the success of the correction will be determined in large measure by how well the underlying diffuse reflection model approximates the actual reflection characteristics of the paint. The model may thus be expected to work better for matte paints (such as FIB7 used at AEDC) than for glossy paints. An extension of the diffuse reflection model has already been undertaken, and is discussed elsewhere.[13]

Appendix: Calculation of *A*-Matrix Coefficients

The grid of the TST model described in Sec. V consisted of about 55,000 points. The coefficient matrix A_{ij} from Eq. (3) thus contains about 3×10^9 entries. Of these, only about 6%, or 1.8×10^8, are nonzero. This is the limiting value in Fig. A1, which shows the number of nonzero pixel numbers N_{ij} from Eq. (7) as a function of the pixel radius N_{map} of the z-buffer projection maps. Figure A2 shows the corresponding maximum error in the self-illumination correction as a function of N_{map}. This error was obtained by calculating the simulated brightness distribution on the test article with a z-buffer radius of 1400 pixels and performing the self-illumination

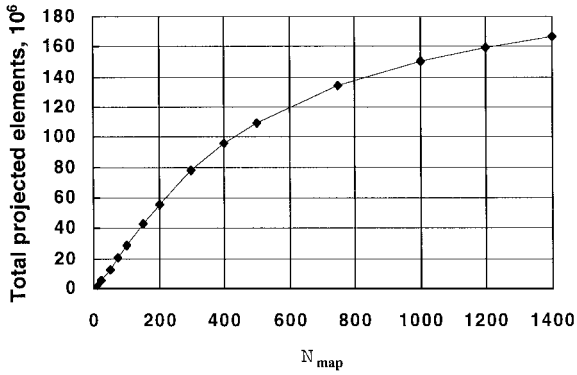

Fig. A1 Number of nonzero projected surface elements vs z-buffer radius.

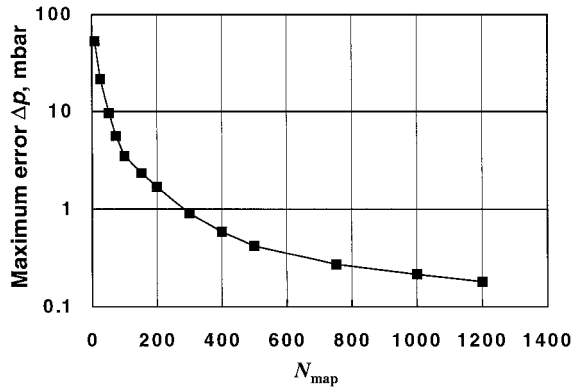

Fig. A2 Correction error vs z-buffer radius.

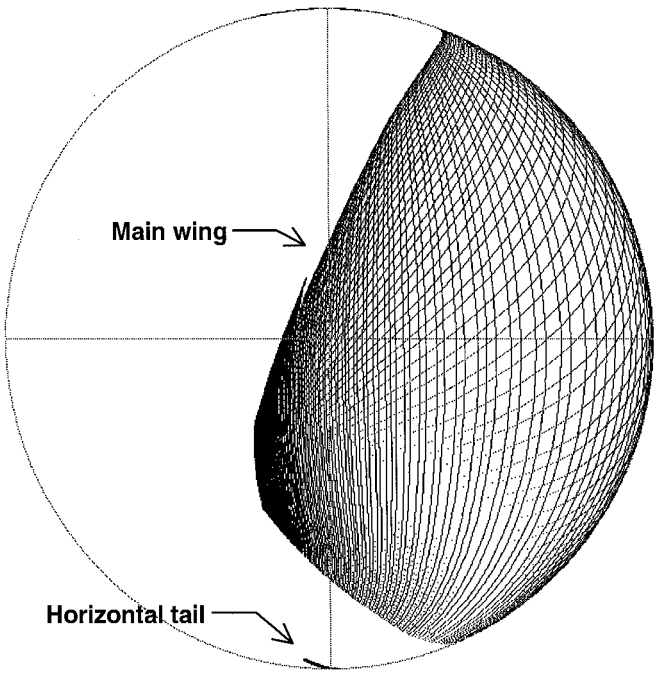

Fig. A3 Graphic example of z-buffer projection map.

correction at the smaller radii indicated in Fig. A2. For $N_{\text{map}} = 300$ pixels, the maximum error is about 1 mbar, even though, according to Fig. A1, only about half of the nonzero projected surface elements are resolved. At this resolution (used in the calculations from Sec. V), the time required to calculate the A matrix was about 90 min on a 400-MHz Intergraph workstation. The size of the resulting A-matrix file was about 320 MB, or about 4 bytes per projected surface element. This storage density was achieved by writing to file, for each surface element index i, only the nonzero N_{ij} pixel counts from Eq. (7), along with the corresponding index j. Both the values N_{ij} and j were stored as 2-byte integers. Calculation of total brightness distributions based on Eqs. (2–4) required about 8 s per iteration, with the majority of time spent reading the stored N_{ij} and j values from file. Figure A3 shows an example of a z-buffer projection map, with a view of the main wing of the TST model from the perspective of a surface element ΔS_i on the fuselage.

Acknowledgments

The TST program was conducted under a Memorandum of Understanding between the U.S. Air Force and the German Ministry of Education, Science, Research, and Technology. We thank our colleagues D. W. Sinclair, M. E. Sellers, and W. L. Sickles for assistance with various aspects of this work.

References

[1]Kavandi, J., Callis, J., Gouterman, M., Khalil, G., Wright, D., Green, E., Burns, D., and McLachlan, B., "Luminescent Barometry in Wind Tunnels," *Review of Scientific Instruments*, Vol. 61, No. 11, 1990, pp. 3340–3347.

[2]Morris, M. J., Donovan, J. F., Kegelman, J. T., Schwab, S. D., Levy, R. L., and Crites, R. C., "Aerodynamic Applications of Pressure Sensitive Paint," *AIAA Journal*, Vol. 31, No. 3, 1993, pp. 419–425.

[3]McLachlan, B. G., and Bell, J. H., "Pressure-Sensitive Paint in Aerodynamic Testing," *Experimental Thermal and Fluid Science*, Vol. 10, No. 4, 1995, pp. 470–485.

[4]Liu, T., Campbell, B. T., Burns, S. P., and Sullivan, J. P., "Temperature- and Pressure-Sensitive Luminescent Paints in Aerodynamics," *Applied Mechanics Reviews*, Vol. 50, No. 4, 1997, pp. 227–246.

[5]Holmes, J. W., "Analysis of Radiometric, Lifetime and Fluorescent Lifetime Imaging for Pressure Sensitive Paint," *Aeronautical Journal*, April 1998, pp. 189–194.

[6]Goss, L. P., Trump, D. D., Sarka, B., Lydick, L. N., and Baker, W. M., "Multi-Dimensional Time-Resolved Pressure-Sensitive-Paint Techniques: A Numerical and Experimental Comparison," AIAA Paper 2000-0832, Jan. 2000.

[7]Liu, T., Guille, M., and Sullivan, J. P., "Accuracy of Pressure Sensitive Paint," AIAA Paper 99-3785, June 1999.

[8]Ruyten, W. M., "Correction of Self-Illumination and Spectral Leakage Effects in Luminescent-Paint Measurements," *Applied Optics*, Vol. 36, No. 14, 1997, pp. 3079–3085.

[9]Ruyten, W. M., "Correcting Luminescent Paint Measurements for Self-Illumination," *ICIASF '97 Record* (International Congress on Instrumentation in Aerospace Simulation Facilities), edited by F. K. Owen, Inst. of Electrical and Electronics Engineers, Piscataway, NJ, 1999, pp. 3–9.

[10]Siegel, R., and Howell, J. R., *Thermal Radiation Heat Transfer,* 2nd ed., McGraw–Hill, New York, 1981, Secs. 7-4, 7-5.

[11]Grum, F., and Becherer, R. J., *Optical Radiation Measurements*, *Vol. 1, Radiometry*, Academic Press, New York, 1979, p. 37.

[12]Nicodemus, F. E., "Directional Reflectance and Emissivity of an Opaque Surface," *Applied Optics*, Vol. 4, No. 7, 1965, pp. 767–773.

[13]Ruyten, W., "Reconstruction of the Net Emission Distribution from the Total Radiance Distribution of a Reflecting Surface," *Journal of the Optical Society of America A*, Vol. 18, No. 1, 2001, pp. 216–223.

[14]Ruyten, W. M., "Self-Illumination Calibration Technique for Luminescent Paint Measurements," *Review of Scientific Instruments*, Vol. 68, No. 9, 1997, pp. 3079–3085.

[15]Emery, A. F., Johansson, O., Lobo, M., and Abrous, A., "A Comparative Study of Methods for Computing the Diffuse Radiation Viewfactors for Complex Structures," *Journal of Heat Transfer*, Vol. 113, No. 2, 1991, pp. 413–422.

[16]Foley, J. D., van Dam, A., Feiner, S. K., and Hughes, J. F., *Computer Graphics: Principles and Practice*, 2nd ed., Addison Wesley, Reading, MA, 1990, Sec. 16-13.

[17]Sillion, F. X., and Puech, C., *Radiosity and Global Illumination*, Morgan Kaufmann, San Francisco, 1994, Chap. 3.

[18]Peterson, J. I., and Fitzgerald, R. V., "New Technique of Surface Flow Visualization Based on Oxygen Quenching of Fluorescence," *Review of Scientific Instruments*, Vol. 51, No. 5, 1980, pp. 670–671.

[19]Morris, M. J., and Donovan, J. F., "Application of Pressure- and Temperature-Sensitive Paints to High-Speed Flows," AIAA Paper 94-2231, June 1994.

[20]Sellers, M. E., and Brill, J. A., "Demonstration Test of Pressure-Sensitive Paint in the AEDC 16-ft Transonic Wind Tunnel Using the TST Model," AIAA Paper 94-2481, June 1994.

J. P. Gore
Associate Editor